LETTER Communicated by Roger Traub

Dynamics of Spiking Neurons with Electrical Coupling

Carson C. Chow
Department of Mathematics, University of Pittsburgh, Pittsburgh, PA 15206, U.S.A.

Nancy Kopell
Department of Mathematics and Center for BioDynamics, Boston University, Boston, MA 02215, U.S.A.

We analyze the existence and stability of phase-locked states of neurons coupled electrically with gap junctions. We show that spike shape and size, along with driving current (which affects network frequency), play a large role in which phase-locked modes exist and are stable. Our theory makes predictions about biophysical models using spikes of different shapes, and we present simulations to confirm the predictions. We also analyze a large system of all-to-all coupled neurons and show that the splay-phase state can exist only for a certain range of frequencies.

1 Introduction

Electrical coupling between neurons has long been thought to have the effect of synchronizing oscillatory neurons, especially if the neurons involved are similar to one another. Here we analyze in more detail the effects of coupling periodically spiking cells by electrical synapses and show that gap junctions can actively foster asynchrony.

We focus on the effects of spike shape and size, along with driving current (which influences the network frequency). Even when the spikes are very thin, the current flow during the spike is shown to have a significant effect on the self-organization of the network, and the current flow during the afterpotentials is an important part of the synchronizing process. Indeed, the frequency of the network plays a significant role in whether the circuit will synchronize, changing the balance of these processes by altering the percentage of time occupied by the spike in a cycle.

We analyze what modes of stable locking are possible for the network and show that synchronization is possible at much higher frequencies than for coupling via inhibitory synapses. However, at very high frequencies, gap junctions can be asynchronizing if the strength of the synapse is sufficiently low; at intermediate frequencies, asynchronous modes can stably exist with the synchronous ones.

The models we use are described by an integrate-and-fire formalism, with the addition of action potentials that are inserted when a cell reaches

threshold. The electrical synapses are modeled as giving currents proportional to the differences in the voltages of the two cells. The analysis is done by means of the spike response method (Gerstner & van Hemmen, 1992; Gerstner, 1995; Gerstner, van Hemmen, & Cowen, 1996; Chow, 1998), in which the effects of the coupling and the spikes are encoded in response kernels. Bressloff and Coombes (1998, 2000) have a similar formalism for analyzing these types of networks. Although the spike response method was invented for synaptic interactions, we show here that it can be used for electrical interactions as well. Indeed the spike response method allows us to consider the simultaneous effects of both kinds of coupling in a uniform formalism. We consider the consequences of the interaction of electrical and inhibitory synapses in a future publication. Here, we consider only electrical coupling and focus on the different effects of spike shape on synchronization in different regimes.

We start in section 2 with the equations of the neurons and the synapses as coupled differential equations. Because the equations are piecewise linear between spikes, they can be explicitly integrated to compute the response kernels. We compute those kernels in terms of the spike parameters, the strength of the electrical synapses, and the intrinsic recovery rate of the uncoupled neuron. This gives explicit solutions for the coupled equations in terms of those parameters and the driving currents to each of the cells (which need not be the same). These explicit solutions are the basis for the analysis in the rest of the article. We note that the solutions have the same form as those analyzed in Chow (1998) describing interactions of cells via synaptic interactions. Thus, the general stability criteria developed there can also be used for the current problem.

In section 3, we consider phase-locked solutions between two spiking neurons connected by gap junctions. We find that, depending on the parameters of the neurons and the gap junction strength, the neurons can either synchronize, antisynchronize, be phase locked at an arbitrary phase, or lose periodic firing. One nonintuitive result is that changing the shape of the spikes may have different effects on the network in different parameter regimes. For example, increasing the amplitude and width of the spikes diminishes the range over which synchrony is stable when the frequency is relatively high. However, at low frequencies in which there is bistability, it can enhance synchrony by diminishing the range of parameters over which the competing antisynchronous solutions are stable.

For nonsynchronous modes such as antisynchrony or splay phase, electrical coupling can change the period of the network. Not only does the period of each cell change in such nonsynchronous modes, but the network period also increases significantly; for example, in the antisynchronous mode, the network frequency is twice that of the cell frequency. Thus, relatively weak electrical coupling may be functionally important in creating appropriate frequency ranges for oscillations in a coupled network. Whether a given mode of locking has a stable existence also depends on the network fre-

quency. The theory predicts a sequence of bifurcations as the driving current to the cells, and hence the frequency of the network, is changed. We test that theory against the two biophysical models and find agreement for a model that has large spikes and another model that has small spikes (see the appendix for details of the models).

In section 4 we consider an all-to-all electrically coupled network of neurons. We show that a large family of periodic phase-locked states can exist, including synchronous and clustered states. We also show that the splay-phase state, in which all the neurons fire in sequence, can exist and be stable over only a finite range of periods. Finally, we review some related modeling work and place our results in the context of physiological systems that are electrically coupled.

2 Equations and Methods

2.1 Spiking Neuron Model. We consider a simple integrate-and-fire model of the neuron with the form

$$C\frac{dV}{d\tilde{t}} = \tilde{I} - g_L V + \sum_l \tilde{A}(\tilde{t} - \tilde{t}^l), \tag{2.1}$$

where V is the voltage, C is the capacitance, $\tilde{I}$ is the applied current, g_L is an effective passive leak conductance, $\tilde{A}(\tilde{t})$ is a term representing spiking and restoring currents, and $\tilde{t}^l$ represents the times that $V(\tilde{t})$ reaches a threshold $V = V_T$ from below. When V reaches threshold, a new term $\tilde{A}(\tilde{t} - \tilde{t}^l)$ is added, which generates a spike (action potential) and resets the potential V to V_0.

The current $\tilde{A}(\tilde{t})$ associated with an individual spike and recovery is chosen to be

$$\tilde{A}(\tilde{t}) = \begin{cases} g_L V_A e^{\tilde{\xi}\tilde{t}}, & 0 < \tilde{t} \le \tilde{\Delta}, \\ -C(V_T - V_0 + V_M)\delta(\tilde{t} - \tilde{\Delta}), & \tilde{\Delta} < \tilde{t}. \end{cases} \tag{2.2}$$

Here V_A is a spiking amplitude scale, $\tilde{\xi}$ is the rise rate of the spiking current, $\tilde{\Delta}$ is the width of the spike from threshold to the peak, V_M is the maximum amplitude above threshold that the spike reaches before the potential is reset, and $\delta(\cdot)$ is the Dirac delta function (which is used to reset the potential). $\tilde{A}(\tilde{t})$ represents nonlinear currents that mediate a fast activation to generate a spike, followed by an even faster inactivation and hyperpolarization to bring the potential back to V_0. V_M is completely determined by the membrane dynamics and $\tilde{A}(\tilde{t})$.

The potential can be shifted and rescaled with $v = (V - V_0)/(V_T - V_0)$ so that the threshold has a value of $v = 1$ and the reset potential is $v = 0$. We

also rescale time by $t = \tilde{t}/\tau_m$, where $\tau_m = C/g_L$. We then arrive at a rescaled system of the form

$$\frac{dv}{dt} = I - v + A(t), \tag{2.3}$$

where

$$I = \frac{(\tilde{I} - g_L V_0)}{g_L(V_T - V_0)}, \tag{2.4}$$

and

$$A(t) = \begin{cases} v_A e^{\xi t}, & 0 < t \le \Delta, \\ -(1 + v_M)\delta(t - \Delta), & \Delta < t, \end{cases} \tag{2.5}$$

with $v_A = V_A/(V_T - V_0)$, $v_M = V_M/(V_T - V_0)$, $\Delta = \tilde{\Delta}/\tau_m$, and $\xi = \tilde{\xi}\tau_m$. The membrane equation has four dimensionless parameters: the applied current I, the spike rise rate ξ, the spike width Δ, and the spike amplitude scale v_A. The latter three parameters control the shape and amplitude of the spike. In this form, I must be larger than unity in order for the potential to reach the threshold for firing.

To compute the scaled maximum amplitude v_M, we integrate equation 2.3 over the width of one spike. Taking initial conditions to be the potential at threshold ($v = 1$ and $t = 0$), we obtain

$$v(t) = 1 + I(1 - e^{-t}) + \frac{v_A}{1 + \xi}[e^{\xi t} - e^{-t}], \quad t < \Delta, \tag{2.6}$$

with v_M defined by $v_M = v(\Delta) - 1$. For a fast-rising and narrow spike (compared to the membrane timescale) we can assume $v_M \simeq v_A e^{\xi\Delta}/(1 + \xi)$. Figure 1 shows four examples of the voltage traces for different parameters of the model given in equation 2.3.

2.2 Spike Response Model for Coupled Neurons. We use the spike response formalism for a system of two neurons coupled with resistive gap junctions. (We can also include synaptic coupling within this formalism.) In doing so, the effects of the gap junction coupling will be separated from the intrinsic dynamics. After the equations are derived, we will apply the techniques previously used to understand the dynamics of synaptically coupled neurons. We will also show how this method can be generalized to a network of N all-to-all coupled neurons.

The equations are

$$\frac{dv_1}{dt} = I_1 - v_1 - g(v_1 - v_2) + \sum_l A(t - t_1^l), \tag{2.7}$$

$$\frac{dv_2}{dt} = I_2 - v_2 - g(v_2 - v_1) + \sum_l A(t - t_2^l), \tag{2.8}$$

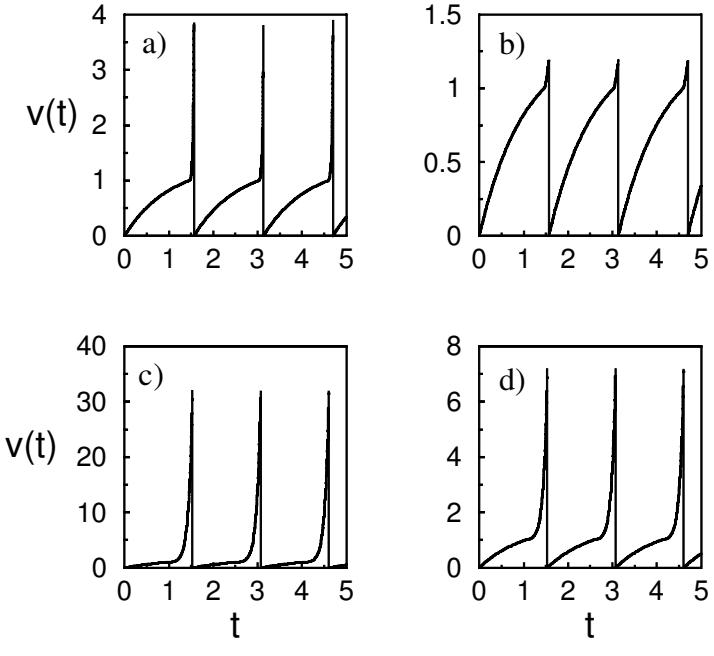

Figure 1: Examples of voltage traces for the integrate-and-fire model with parameters (a) $\xi = 50, \Delta = 0.1, v_A = 1, I = 1.3$, (b) $\xi = 12, \Delta = 0.1, v_A = 1, I = 1.3$, (c) $\xi = 12, \Delta = 0.5, v_A = 1, I = 1.55$, (d) $\xi = 12, \Delta = 0.5, v_A = .1, I = 1.55$.

where g is a gap junction strength (scaled by g_L) and t_i^l represents the times when v_i crosses the threshold from below. The spiking kernel $A(t)$ generates a spike and resets the potential to zero. Our strategy is to express the dynamics for v_i in terms of a set of response kernels, which we will explicitly calculate.

We first transform into normal modes $v_+ = v_1 + v_2$ and $v_- = v_1 - v_2$ to obtain

$$\frac{dv_+}{dt} = I_+ - v_+ + \sum_l A(t - t_1^l) + \sum_m A(t - t_2^m) \tag{2.9}$$

$$\frac{dv_-}{dt} = I_- - rv_- + \sum_l A(t - t_1^l) - \sum_m A(t - t_2^m), \tag{2.10}$$

where $r = 1 + 2g$, $I_+ = I_1 + I_2$ and $I_- = I_1 - I_2$. Integrating gives

$$v_+ = I_+(1 - e^{-t}) + \sum_l \eta_+(t - t_1^l) + \sum_m \eta_+(t - t_2^m), \tag{2.11}$$

$$v_- = \frac{I_-}{r}(1 - e^{-rt}) + \sum_l \eta_-(t - t_1^l) - \sum_m \eta_-(t - t_2^m). \tag{2.12}$$

Since we are interested in the steady state, we can start the interaction at any initial conditions; we have taken initial conditions of $v_+ = v_- = 0$.

The kernels are nonzero only for positive argument. They are given by

$$\eta_\alpha(t) = \int_0^t e^{-r_\alpha(t-t')} A(t')dt', \tag{2.13}$$

and after integrating

$$\eta_\alpha(t) = \begin{cases} v_A(r_\alpha + \xi)^{-1}[e^{\xi t} - e^{-r_\alpha t}], & 0 < t \le \Delta \\ -(1 + v_M - \eta_\alpha(\Delta))e^{-r_\alpha(t-\Delta)}, & \Delta < t, \end{cases} \tag{2.14}$$

where $\alpha = \pm$, $r_+ = 1$ and $r_- = r$. We note that for fast-rising and narrow spikes, $v_M \simeq \eta_+(\Delta)$.

Returning to the original coordinates and assuming that the neurons have been spiking for a long time so that initial conditions have decayed away, we obtain the spike response equations,

$$v_1(t) = \hat{I}_1 + \sum_l \gamma_s(t - t_1^l) + \sum_m \gamma_c(t - t_2^m), \tag{2.15}$$

$$v_2(t) = \hat{I}_2 + \sum_l \gamma_s(t - t_2^l) + \sum_m \gamma_c(t - t_1^m), \tag{2.16}$$

where

$$\hat{I}_1 = \frac{1}{2}\left[\left(1 + \frac{1}{r}\right)I_1 + \left(1 - \frac{1}{r}\right)I_2\right], \tag{2.17}$$

$$\hat{I}_2 = \frac{1}{2}\left[\left(1 - \frac{1}{r}\right)I_1 + \left(1 + \frac{1}{r}\right)I_2\right], \tag{2.18}$$

and

$$\gamma_s = \frac{1}{2}[\eta_+(t) + \eta_-(t)], \tag{2.19}$$

$$\gamma_c = \frac{1}{2}[\eta_+(t) - \eta_-(t)]. \tag{2.20}$$

γ_s is the spike generation and reset kernel and γ_c is the coupling kernel in the spike response method (Gerstner et al., 1996; Chow, 1998). We note that $\sum_m \gamma_c(t - t_i^m)$ can be interpreted as the contribution to the membrane potential due to the gap junction coupling. It is the gap junction analog of the postsynaptic potential.

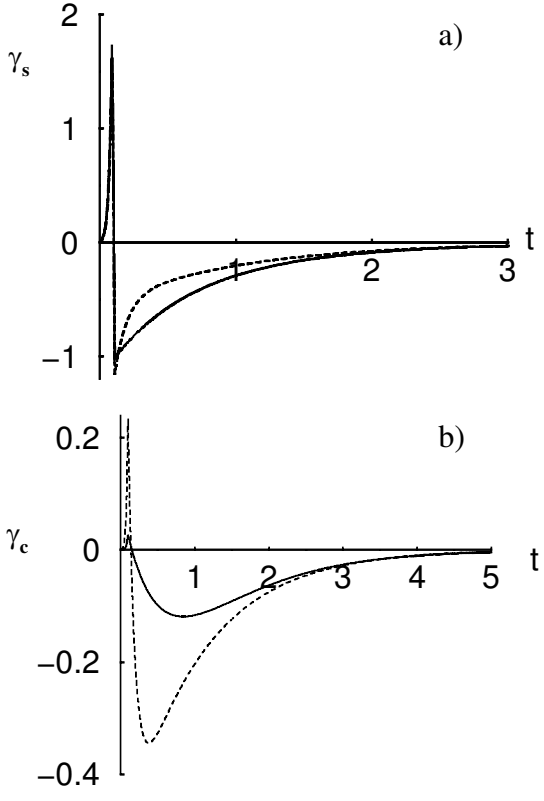

Figure 2: (a) Two examples of the γ_s kernel with parameters $\Delta = 0.1$, $\xi = 50$, $v_A = 1$, and gap junction conductances $g = 0.5$ (solid line) and $g = 5$ (dashed line). (b) Two examples of the γ_c kernel with $\Delta = 0.1$, $\xi = 50$, $v_A = 1$, and gap junction conductances $g = .5$ (solid line) and $g = 5$ (dashed line).

Written out explicitly, the γ_s kernel is given by

$$\gamma_s(t) = \begin{cases} \frac{v_A}{2}\left[(1+\xi)^{-1}[e^{\xi t} - e^{-t}] + (r+\xi)^{-1}[e^{\xi t} - e^{-rt}]\right], & 0 < t \le \Delta \\ -\frac{1}{2}\left[e^{-(t-\Delta)} + \delta_c e^{-r(t-\Delta)}\right], & \Delta < t, \end{cases} \tag{2.21}$$

where

$$\delta_c = 1 + 2\gamma_c(\Delta). \tag{2.22}$$

The γ_s kernel has the shape of a single spike as seen in Figure 2a. Increasing the gap junction strength through r mainly affects the recovery phase.

The γ_c kernel is given by

$$\gamma_c(t) = \begin{cases} \frac{v_A}{2}\left[(1+\xi)^{-1}[e^{\xi t} - e^{-t}] - (r+\xi)^{-1}[e^{\xi t} - e^{-rt}]\right], & 0 < t \le \Delta \\ -\frac{1}{2}\left[e^{-(t-\Delta)} - \delta_c e^{-r(t-\Delta)}\right], & \Delta < t. \end{cases} \tag{2.23}$$

The γ_c kernel is the contribution to the electrical coupling due to a single spike. Examples of γ_c are shown in Figure 2b. For short times, γ_c is positive, rising until a cusp, which occurs at the peak of the spike. After the cusp, γ_c begins to decrease, becoming negative for long times. The sum over the γ_c kernels can be thought of as setting a background potential level on which the spiking takes place.

The parameter δ_c, a measure of the maximum amount of excitatory input received, is important for controlling the background potential level. Later, it will be seen that δ_c is the critical parameter for determining the synchronizing behavior of the network. For fast-rising spikes, we can assume $\exp(\xi\Delta) \gg \exp(-\Delta)$, leading to

$$\delta_c \simeq 1 + v_M\left(1 - \frac{1+\xi}{r+\xi}\right), \tag{2.24}$$

where we have used $v_M \equiv \eta_+(\Delta) \simeq v_A e^{\xi\Delta}/(1+\xi)$. δ_c can be increased by increasing r through the gap junction strength g or increasing the maximum spike amplitude v_M. (Note that v_M is measured in reference to a fixed post-spike hyperpolarization.) While increasing the spike rise rate ξ increases v_M, if v_M is kept fixed, increasing ξ actually decreases δ_c. For weak coupling strength ($g \ll 1$), δ_c has the form

$$\delta_c \simeq 1 + \frac{2gv_M}{1+\xi}. \tag{2.25}$$

In the ensuing text, we will refer to spikes with $\delta_c \gg 1$ as large spikes and spikes with $\delta_c \sim 1$ as small spikes.

3 Phase-Locked States

In this section we apply the formalism of the previous section and analyze the existence and stability of phase-locked states for two neurons coupled through gap junctions. We focus on the states of synchrony (S) and antisynchrony (AS), although a third phase-locked state can also exist. We show that by changing the frequency of the network, the neurons can make transitions between these phase-locked states. In some instances, bistability is possible.

3.1 Conditions for Periodic Phase Locking. We are interested in the existence and stability of phase-locked periodic solutions. Here, we describe

a self-consistent method for determining the period T of a periodic solution and the phase difference ϕ between the cells in that periodic solution. We show that there is a function $G(\phi, T)$ whose zeros for fixed T give the phase difference; there is a companion equation that is used to determine T.

We consider two neurons firing in a phase-locked pattern. We analyze this situation by supposing that the neurons fire periodically at $t_1^l = -lT$ and $t_2^l = (\phi - l)T$. Without loss of generality, we assume that cell 1 is ahead of or at the same position as cell 2, that is, $\phi \geq 0$. The next time the ith neuron fires is when the potential v_i reaches threshold from below (i.e., $\dot{v}_i > 0$). Thus, using the spike response equations, we can derive a condition for phase-locked firing. Noting that neuron 1 will next fire at $t = 0$ and neuron 2 will next fire at $t = \phi T$, we obtain from equations 2.15 and 2.16

$$v_1(0) = 1 = \hat{I}_1 + \sum_{l \geq 1} \gamma_s(lT) + \sum_{l \geq 1} \gamma_c(lT - \phi T,) \tag{3.1}$$

$$v_2(\phi T) = 1 = \hat{I}_2 + \sum_{l \geq 1} \gamma_s(lT) + \sum_{l \geq 0} \gamma_c(lT + \phi T). \tag{3.2}$$

This is a set of two equations with two unknowns. Note that the second sum in equation 3.2 starts with the index $l = 0$ because cell 2 feels the effect of cell 1 in the first cycle, but not vice versa.

We can rewrite this system in a more convenient form. Subtracting equation 3.2 from 3.1 yields

$$G(\phi, T) = \widehat{I}_1 - \widehat{I}_2 = \frac{I_1 - I_2}{1 + 2g}, \tag{3.3}$$

where

$$G(\phi, T) = \gamma_c(\phi T) + \sum_{l \geq 1} [\gamma_c(lT + \phi T) - \gamma_c(lT - \phi T)]. \tag{3.4}$$

This equation can be interpreted as a condition for the phase ϕ given a fixed period T (provided a solution with that T is possible). Adding equation 3.2 to 3.1 and dividing by two yields

$$F(\phi, T) = 1 - \bar{I}, \tag{3.5}$$

where

$$F(\phi, T) = \frac{1}{2}\gamma_c(\phi T) + \sum_{l \geq 1} \left[\gamma_s(lT) + \frac{1}{2}(\gamma_c(lT - \phi T) + \gamma_c(lT + \phi T)) \right] \tag{3.6}$$

and $\bar{I} = (\widehat{I}_1 + \widehat{I}_2)/2 = (I_1 + I_2)/2$. This equation gives a condition for the period T given a fixed phase ϕ.

Although equation 3.5 could possibly allow multiple solutions for a given phase ϕ, there is only one "physical" solution, which is given by the smallest solution for T. This is because the neuron is considered to fire and reset immediately on crossing the threshold from below. A condition that also must be satisfied is that a neuron must remain subthreshold throughout its period. We examine this condition in detail for AS in section 3.3.

For homogeneous systems ($I_1 = I_2$) S ($\phi = 0$) and AS ($\phi = 0.5$) both satisfy equation 3.3. For S, the period condition, equation 3.5, is the same as that for a single neuron. As we will show in section 3.2, a solution to equation 3.5 can almost always be found for S. However, the existence of AS is not guaranteed. As will be shown in section 3.3, a neuron may not remain subthreshold while the other neuron fires.

Stability of these periodic phase-locked solutions can also be analyzed. In Chow (1998), a sufficient condition and a separate necessary condition for stable phase locking were derived. The sufficient condition for stability of a locked solution with phase ϕ is that the slopes of the kernels (γ_s and γ_c) are both positive at times $t = lT \pm \phi T$; that is, they are rising at the time of firing (Gerstner et al., 1996; Chow, 1998). The necessary condition for stability is that the derivative of $G(\phi, T)$ with respect to ϕ must be positive (van Vreeswijk, Abbott, & Ermentrout, 1994; Chow, 1998).

3.2 Period of Phase Locking. The network period depends on the parameters and the phase-locked state. For a given fixed phase ϕ, the period T is determined implicitly from equation 3.5. Here we will show that for S, a solution for the period can always be found if the input current is suprathreshold and not too large. However, for AS, condition 3.5 may not always have a solution for T. We show that if I is too small (depending on the other parameters), there is no solution, implying that AS does not exist in that regime. As will be seen in section 3.3, even if a solution exists to equation 3.5, AS still may not exist if the value obtained for the period is too large.

When both S and AS exist, we analyze equation 3.5 to see the relationship between their periods, T_S and T_{AS}, respectively. The result is that for large spikes, $T_{AS} < T_S$ for fixed parameter values, but the opposite is true for small spikes. We also look at how the period changes with parameters. We show that increasing the gap junction strength g decreases T_{AS} for large spikes, but increases it for small spikes. Since equation 3.5 is a continuous function of ϕ, T changes continuously with changing ϕ.

For S, using equations 2.19 and 2.20, equation 3.6 becomes

$$F(0, T_S) = \sum_{l \geq 1} \eta_+(lT_S). \tag{3.7}$$

Inserting the kernel η_+ from equation 2.14 into 3.7 and evaluating the sums, condition 3.5 becomes

$$F(0, T_S) = \frac{e^{\Delta}}{1 - e^{T_S}} = 1 - \bar{I} \tag{3.8}$$

for $T_S > \Delta$. It can be easily shown that this is the period condition for an uncoupled neuron (Chow, 1998; Chow, White, Ritt, & Kopell, 1998). The period is defined implicitly by equation 3.8.

The function $F(0, T_S)$ is negative and monotone increasing in T_S. For $1 < \bar{I} \leq 1 + (1 - e^{\Delta})^{-1}$ there is always a solution for T_S. (We note that the period is well defined only for $T_S > \Delta$.) Solving equation 3.8 for T_S yields

$$T_S = \ln\left(\frac{\bar{I} - 1 + e^{\Delta}}{\bar{I} - 1}\right). \tag{3.9}$$

The threshold for firing is $\bar{I} = 1$. The period decreases with increasing $\bar{I}$.

For AS, equation 3.6 gives

$$F(1/2, T_{AS}) = \sum_{l \geq 1} \gamma_s(lT_{AS}) + \sum_{m \geq 0} \gamma_c(mT_{AS} + T_{AS}/2). \tag{3.10}$$

Inserting the kernels 2.21 and 2.23 for $t > \Delta$ into equation 3.10 and evaluating the sums leads to the period condition equation 3.5:

$$F(1/2, T_{AS}) = \frac{\delta_c}{2} \frac{e^{r\Delta}}{e^{rT_{AS}/2} + 1} - \frac{1}{2} \frac{e^{\Delta}}{e^{T_{AS}/2} - 1} = 1 - \bar{I}. \tag{3.11}$$

for $T_{AS} > 2\Delta$. The smallest T_{AS} satisfying equation 3.11 is the only physical solution.

There are situations where a solution to equation 3.11 does not exist. From that equation, we see that for a given $\bar{I}$, for δ_c large enough and r small enough, then T_{AS} does not exist since $F(1/2, T_{AS})$ stays above $1 - \bar{I}$. By the same reasoning, solutions for T_{AS} can then exist for subthreshold input ($\bar{I} < 1$); the excitation provided by each neuron through the gap junction would sustain firing.

Except for cases where δ_c and r are very large, near the smallest solution of equation 3.11, we have $\partial F(1/2, T_{AS})/\partial T > 0$. This implies that increasing $\bar{I}$ decreases the period. From equation 3.11 we see that increasing δ_c increases $F(1/2, T_{AS})$ and thus decreases T_{AS}. This can be understood heuristically since the spike contributes an effective excitation through the gap junction and δ_c increases with increasing width and amplitude of the spike. We note that δ_c increases when $r = 1 + 2g$ increases. On the other hand, the factor $e^{r\Delta}/(e^{rT_{AS}/2} + 1)$ increases only if $T_{AS} < 2\Delta$ and decreases otherwise. However, for relatively small r and T_{AS} (recall that small is in comparison to the effective leak time), the factor decreases slowly. Thus, for cells with large spikes and periods that are fast compared to the leak time, increasing r generally decreases the period for AS, while for cells with small spikes and long periods, increasing r increases the period.

We can compare the periods of AS to S by rewriting $F(1/2, T)$ as

$$F(1/2, T) = F(0, T) + \psi(T) \tag{3.12}$$

where

$$\psi(T) = \frac{\delta_c}{2}\frac{e^{r\Delta}}{e^{rT/2}+1} - \frac{1}{2}\frac{e^{\Delta}}{e^{T/2}+1}\,. \tag{3.13}$$

Comparing to equation 3.8, we find $T_S = T_{AS}$ when $\psi = 0$. For a given period, there is a set of possible parameters δ_c and r for which $\psi = 0$. The trivial solution is $\delta_c = 1$ and $r = 1$, which corresponds to uncoupled neurons. For weak coupling and a small spike amplitude, $T_S \sim T_{AS}$. If $\psi > 0$, then $T_S > T_{AS}$, and vice versa. From equation 3.13, we find that ψ can be positive if δ_c is large enough. Again, this can be understood heuristically. For strong spikes and weak coupling, AS has a shorter period, but for weak spikes and strong coupling, the opposite is true.

3.3 Existence of the Antisynchronous State. In order for AS to exist, the potential of the neurons must remain below threshold for the duration of a period. This can be violated if the spikes have large enough amplitude or the electrical coupling is strong enough so that when one of the neuron spikes, it induces the second neuron to cross threshold; that is, as soon as one of the neurons fires, the other will be induced to fire nearly immediately and the neurons will tend to synchronize. This effect is similar to fast threshold modulation (Somers & Kopell, 1993). The spike mediated through the gap junction acts like a brief excitatory pulse synchronizing the two neurons, prohibiting antisynchrony.

We can make this more concrete by considering AS where $t_1^l = -lT$ and $t_2^l = T/2 - lT$. The potential of neuron 1 obeys

$$v_1(t) = I_1 + \sum_{l\geq 0}[\gamma_s(t + lT) + \gamma_c(t - T/2 + lT)], \quad t > 0. \tag{3.14}$$

We require $v_1(t) < 1$ for $0 < t < T$. When the spike of neuron 2 is felt by neuron 1 at $t = T/2 + \Delta$, there is a chance that neuron 1 may be induced to fire. To prevent this, we must have

$$v_1(T/2 + \Delta) = I_1 + \sum_{l\geq 0}[\gamma_s(T/2 + \Delta + lT) + \gamma_c(\Delta + lT)] < 1. \tag{3.15}$$

Using equations 2.21 and 2.23 in 3.15 and evaluating the sums yields

$$\delta_c < \left(3 - 2I_1 + \frac{1}{e^{T/2}-1}\right)(1 + e^{-rT/2}). \tag{3.16}$$

The applied current and the period are related through condition 3.11. For homogeneous neurons, $I_1 = \bar{I}$. Solving equation 3.11 for $\bar{I}$ and substituting into 3.16 yields

$$\delta_c < \left(1 + \frac{1 - e^{\Delta}}{e^{T/2}-1} + \frac{\delta_c e^{r\Delta}}{e^{rT/2}-1}\right)(1 + e^{-rT/2}). \tag{3.17}$$

For very narrow spikes ($\Delta \simeq 0$), this inequality is approximately

$$\delta_c < \frac{\sinh rT/2}{\sinh rT/2 - 1}. \tag{3.18}$$

As the period T increases, the right-hand side of equation 3.18 decreases toward unity. Hence, as the period gets longer, δ_c must be smaller in order for AS to exist. In the limit of $T \to \infty$, condition 3.18 becomes $\delta_c < 1$. Recall that $\delta_c \geq 1$ and decreases with decreasing spike amplitude. Thus, as the period approaches infinity, the spike amplitude must approach zero for AS to exist. The behavior is the same for increasing the gap junction strength r. For a fixed spike amplitude and gap junction strength, there is a maximum period allowable for AS to exist. The larger the spike or stronger the gap junction, the smaller this maximum is.

3.4 Global Behavior. A global view of the existence and stability of phase-locked states can be obtained from condition 3.3 if we treat the period T as a bifurcation parameter. For a fixed period T, equation 3.3 provides the phase ϕ of any locked solution; by Chow (1998), that solution is unstable if the slope of $G(\phi, T)$ is negative. In section 3.7, we relate the bifurcation unfolding for T to the network parameters I and g.

We can compute $G(\phi, T)$ explicitly by evaluating the sums in equation 3.4 to obtain for $T \geq 2\Delta$

$$G(\phi, T) = \gamma_c(\phi T) - \frac{1}{2}\left[\frac{e^{-(T+\phi T-\Delta)} - e^{-(T-\phi T-\Delta)}}{1-e^{-T}} - \delta_c \frac{e^{-r(T+\phi T-\Delta)} - e^{-r(T-\phi T-\Delta)}}{1-e^{-rT}}\right], \quad \phi T \leq \Delta, \tag{3.19}$$

$$G(\phi, T) = -\frac{1}{2}\left[\frac{e^{-(\phi T-\Delta)} - e^{-(T-\phi T-\Delta)}}{1-e^{-T}} - \delta_c \frac{e^{-r(\phi T-\Delta)} - e^{-r(T-\phi T-\Delta)}}{1-e^{-rT}}\right], \quad \Delta < \phi T, < T/2, \tag{3.20}$$

and $G(\phi, T)$ is an odd function about $\phi = 1/2$. The functional form for G for $T < 2\Delta$ is much more complicated.

Four examples of $G(\phi, T)$ versus ϕ for a progression of different fixed periods T are shown in Figure 3. Phase-locked solutions are given by the zero crossings of $G(\phi, T)$. If the slope at the zero crossing is negative, then the solution is unstable. Although the condition $G'(\phi, T) > 0$ is a necessary condition only for stability, it allows us to use the graphs of G to give insight into the regimes for which various locked solutions are stable. Bifurcations take place at critical points T_C that satisfy $G(\phi, T_C) = 0$. The four parts of Figure 3 capture the qualitative dynamics of a system coupled with weak gap junctions. The bifurcation sequence is summarized in Figure 4. For

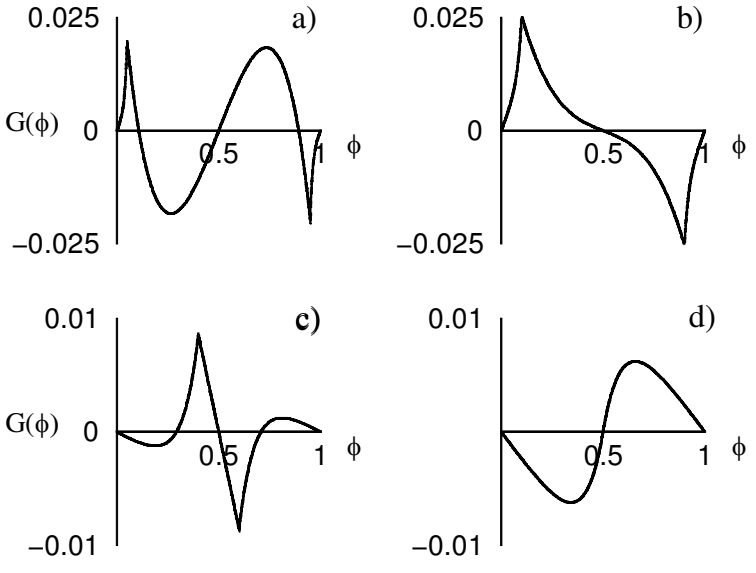

Figure 3: Four examples of $G(\phi)$ with parameters $\Delta = 0.1, \xi = 50, g = .5, v_A = 1$ and period (a) $T = 2$, (b) $T = 1$, (c) $T = 0.25$, and (d) $T = 0.2$.

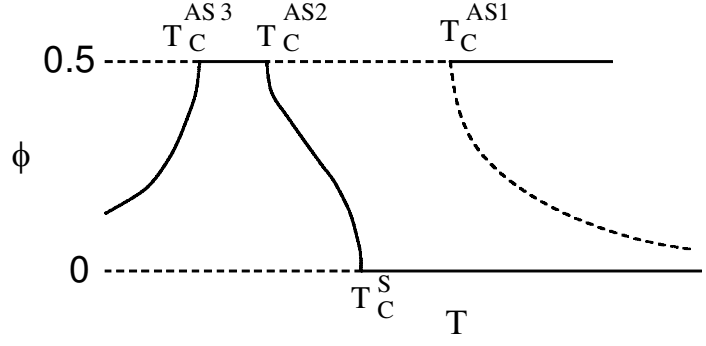

Figure 4: Bifurcation sequence for phase-locked states with phase ϕ and period T for weak gap junctions. Solid lines indicate stable states and dashed lines unstable states. Moving from left to right corresponds to increasing period, and moving from right to left corresponds to increasing frequency. There are four bifurcation points: T_C^{AS1}, T_C^{AS2}, T_C^{AS3}, and T_C^{S}.

strong gap junctions, synchrony is always stable, as one would expect. As the gap junction strength is reduced, the state will make a transition into the corresponding weak gap junction state for that particular period.

We consider the bifurcation unfolding for weak gap junctions as the period is decreased (see Figure 4). For a long period, as in Figure 3a, both $\phi = 0$ and $\phi = 0.5$ are zeros with $G'(\phi, T) > 0$. Thus, the necessary conditions for stable S and AS are satisfied. However, AS may not exist for long periods, as shown in section 3.3. There is also an unstable third mode that appears symmetrically around AS. (This third mode also exists for synaptic coupling; van Vreeswijk et al., 1994; Hansel, Mato, & Meunier, 1995; Chow, 1998.) $G(\phi, T)$ has a cusp between $\phi = 0$ and the third mode, which comes from the cusp in γ_c. As the period is decreased, the third mode approaches $\phi = 0.5$ until an inverse pitchfork bifurcation at $G'(0.5, T) = 0$, when AS loses stability and the third mode disappears (see Figure 3b). This corresponds to the value T_C^{AS1} in Figure 4. With a further decrease in period, S loses stability through a pitchfork bifurcation, and a stable third mode reappears (see Figure 3c). This occurs at T_C^S in Figure 4. As the period decreases even further, the cusp approaches $\phi = 0.5$. At $T = T_C^{AS2} \equiv 2\Delta$, the cusp crosses $\phi = 0.5$, and stable AS appears (see Figure 3d). This bifurcation is discontinuous because of the cusp. For a smooth spike, the cusp would be smoothed and the AS would gain stability through a pitchfork bifurcation. For even shorter periods, as will be seen in section 3.6, the AS state can lose stability to the third mode at T_C^{AS3}.

In the synchronous state, the period of the network is given by their intrinsic dynamics because the effect of the electrical coupling is zero. For AS, the contribution from the electrical coupling affects the period (although this effect may be small). In the two following sections, we show how the critical points change as the network parameters are varied. We also consider the sufficient conditions for stability of S and AS in these sections. With these results and those of section 3.2, we can construct the bifurcation sequence for changes in the applied current I and the gap junctional strength g. This bifurcation diagram gives information about necessary conditions for the stability of S and AS. In the next two sections we also consider the sufficient conditions.

3.5 Synchrony. As seen in section 3.4, S can become unstable if the period is too short. From equation 3.4 we find

$$G'(0, T)/T = \dot{\gamma_c}(0) + 2\sum_{l\geq 1} \dot{\gamma_c}(lT), \tag{3.21}$$

where the prime indicates a derivative with respect to ϕ and the dot indicates the derivative with respect to t. For γ_c given by equation 2.23, $\dot{\gamma_c}(0) = 0$. This reflects the fact that the neurons do not immediately affect each other upon firing. Inserting equation 2.23 into 3.21 and evaluating the sum, we find that for $T > \Delta$,

$$G'(0, T)/T = \frac{e^{\Delta}}{e^{T} - 1} - \delta_c \frac{re^{r\Delta}}{e^{rT} - 1}\,. \tag{3.22}$$

Note that $\delta_c > 1$ since $\gamma_c(\Delta) > 0$ and $r > 1$. Thus, for T small enough, δ_c large enough, and r not too large, the second term will dominate the first term in equation 3.22, and $G'(0, T)$ will become negative, indicating the instability of S.

The lower bound of the period for stable S is given by the critical period T_C^S, which satisfies $G'(0, T_C^S) = 0$. For T below T_C^S, the necessary condition for stability is violated, and stable S cannot exist. We examine how T_C^S behaves when we change the parameters. The critical condition (see equation 3.22) can be rearranged to take the form

$$\frac{e^{rT_C^S} - 1}{e^{T_C^S} - 1} = r\delta_c e^{(r-1)\Delta}. \tag{3.23}$$

For large r, T_C^S decreases with increasing r. Thus for very strong gap junctions, the lower bound is the width of the spike, implying that synchrony can be stable at any allowable period (periods smaller than the width of the spike are not allowable in our model). This synchronizing tendency is the general presumption of gap junctions. However, if the gap junction is not strong, then there can be a range of frequencies for which S is unstable. The left-hand side of equation 3.23 is monotone increasing in T_C^S. Thus, T_C^S increases with increasing δ_c or Δ. The conditions for stable synchrony depend importantly on the spike width Δ and on δ_c. As either of these is increased, a longer period (lower frequency) is required for stable S. A larger-amplitude spike leads to a larger δ_c and hence makes it more difficult to synchronize two neurons in the sense that the range of frequencies where they can synchronize is reduced.

We now consider sufficient conditions for stability. In Chow (1998), it was shown that $\dot{\gamma}_s(lT) > 0$, $\dot{\gamma}_c(0) \geq 0$, and $\dot{\gamma}_c(mT) > 0$, for $l \geq 0$, $m \geq 1$, was sufficient for stability. From equation 2.21 and Figure 2a, the slope of γ_s is always positive. From equation 2.23 and Figure 2b, the slope of $\gamma_c(lT)$ is negative between the maximum at $t = \Delta$ and the minimum $t = t_{\min}$ but positive everywhere else. Minimizing equation 2.23 for $t > \Delta$ gives

$$t_{\min} = \Delta + \frac{1}{2g} \ln \delta_c(1 + 2g). \tag{3.24}$$

Recall that $\dot{\gamma}_c(0) = 0$. For $T > t_{\min}$, we have $\dot{\gamma}_c(mT) > 0$, ensuring stability. For $T < t_{\min}$, the slope of $\gamma_c(T)$ can be negative, and stability is no longer ensured. (Note that $T > \Delta$; the period must be longer than the width of a spike.) For strong gap junctions, $t_{\min}$ approaches Δ. This implies that as the gap junction becomes stronger, S is guaranteed to be stable at higher and higher frequencies.

For $g \ll 1$, we can use equation 2.25 for δ_c in 4.24 and expand to obtain

$$t_{\min} \simeq \Delta + 1 + \frac{v_M}{1 + \xi}. \tag{3.25}$$

Thus, for weak gap junction strength, g has no effect on $t_{\min}$ at linear order.

3.6 Antisynchrony. The behavior of $G(\phi, T)$ indicates that AS could be stable for either long periods or very short periods. We now investigate these possibilities in more detail. A necessary condition for stability of AS is that $G'(0.5, T) > 0$. The sufficient conditions for stability are given by $\dot{\gamma}_s(lT + T/2) > 0$ and $\dot{\gamma}_c(lT + T/2) > 0$.

From equation 3.4, we find that

$$G'(0.5, T)/T = 2 \sum_{l \geq 0} \dot{\gamma}_c(lT + T/2). \tag{3.26}$$

After evaluating the sum, we obtain

$$G'(0.5, T)/T = \begin{cases} 2\dot{\gamma}_c(T/2) + \frac{e^{-(3T/2-\Delta)}}{1-e^{-T}} - \delta_c r \frac{e^{-r(3T/2-\Delta)}}{1-e^{-rT}}, & T \leq 2\Delta \\ \frac{e^{-(T/2-\Delta)}}{1-e^{-T}} - \delta_c r \frac{e^{-r(T/2-\Delta)}}{1-e^{-rT}}, & T > 2\Delta\,, \end{cases} \tag{3.27}$$

where

$$\dot{\gamma}_c(T/2) = \frac{v_A}{2}\left[\frac{\xi e^{\xi T/2} + e^{-T/2}}{1+\xi} - \frac{\xi e^{\xi T/2} + r e^{-rT/2}}{r+\xi}\right], \qquad T \leq 2\Delta\,. \tag{3.28}$$

First consider the behavior for $T \leq 2\Delta \equiv T_C^{AS2}$. This is the situation where the spikes are overlapped; one neuron reaches threshold, while the other neuron is still in a spiking phase. From equation 4.27 and as seen in Figure 3d, AS can be stable for $T = T_C^{AS2}$, provided r is small enough. However, $\dot{\gamma}_c(0) = 0$ and is monotone, increasing in T until $T = 2\Delta$. Thus, if T is reduced, there is a bifurcation at T_C^{AS3} when $G'(0.5, T_C^{AS3}) = 0$, (not shown in Figure 3). Stability of AS is possible for $T_C^{AS3} < T \leq T_C^{AS2}$. For small r, increasing r will increase T_C^{AS3}. Thus, the regime for stable AS at these short periods is reduced and could possibly be eliminated by increasing the gap junction strength.

The sufficient conditions for stability are satisfied if $T/2 > t_{\min}$, where $t_{\min}$ is given in equation 3.24. This sets a minimum on the period that depends on δ_c. In the short period regime, we have shown that AS could satisfy the necessary condition for stability when the period is reduced to less than twice the width of the spike. However, at this point, the sufficient conditions are not satisfied since $T/2 < \Delta < t_{\min}$. Although stable solutions are possible if the sufficient condition is violated, it may be that for extremely high frequencies, neither S nor AS is stable.

For T slightly larger than 2Δ, $G'(0.5T)$ is negative. Once the spikes are no longer overlapped, AS immediately loses stability. This bifurcation is seen in Figures 3c and 3d. The bifurcation is discontinuous because the

spike shapes are not smooth. Had a smoother spike shape been chosen, the transition from stability to instability would be continuous.

As the period is increased, the necessary condition for AS stability begins to be satisfied at the critical period T_C^{AS1} satisfying $G'(0.5, T_C^{AS1}) = 0$. Thus, T_C^{AS1} gives a lower bound for stable AS in the long period regime ($T > 2\Delta$). Applying this to equation 4.27 for this regime gives the following condition for this lower bound:

$$\frac{\sinh(rT_C^{AS1}/2)}{\sinh(T_C^{AS1}/2)} = r\delta_c e^{(r-1)\Delta}. \tag{3.29}$$

The left-hand side of equation 4.29 is monotone increasing in T_C^{AS1}, so increasing δ_c or Δ increases T_C^{AS1}. Thus, large spikes increase the lower bound on period for stable AS in the long period range.

For strong gap junctions, T_C^{AS1} decreases and in the limit $r \to \infty$, $T_C^{AS1} \to 2\Delta$. The maximum period allowed for existence of AS as given by equation 3.18 also decreases as r is increased and at a slightly faster rate. This implies that as the gap junction strength increases, AS can be stable at shorter periods in the long period regime, although it likely loses existence before the period can get too short.

To summarize, the necessary condition for stability of AS is satisfied for periods longer than T_C^{AS1} provided the gap junction is not too strong. It is also satisfied for short periods between T_C^{AS3} and T_C^{AS2}, although the sufficient conditions are not satisfied. This region is reduced with increasing gap junction strength. For long periods, existence is lost if the gap junction is too strong or the period is too long. Results from section 3.5 lead to the conclusion that in the short period regime, large spikes diminish the range of periods over which synchrony is stable. From this section we see that in the long period regime, large spikes diminish the range over which AS is stable. These results are borne out in numerical solutions, as will be shown in section 3.9.

3.7 Bifurcations for I and g. In section 3.4, we showed that for weak gap junctions, a bifurcation sequence shown in Figure 4 takes place for changes in the period T. We now relate this sequence to bifurcations, using as parameters the applied current I and gap junction strength g. This is accomplished by identifying the locations of the four bifurcation points: T_C^{AS1}, T_C^{AS2}, T_C^{AS3}, and T_C^S.

From section 3.2 we showed that increasing the applied current I decreases the period T. Thus, moving from right to left on the bifurcation plot in Figure 4 corresponds to increasing I. However, for a fixed I, the states S, AS, or third mode will have different periods, so the diagram will not carry over directly. The bifurcation sequence will vary according to whether the period decreases or increases as the phase of the periodic locked state moves

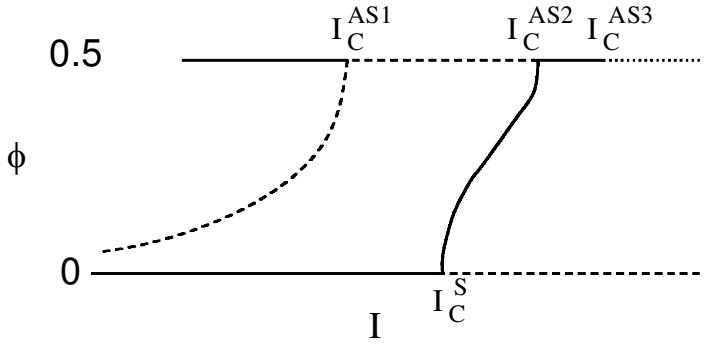

Figure 5: Bifurcation sequence for phase-locked states with phase ϕ and applied current I for large spikes. Solid lines indicate stable states, dashed lines unstable, and dotted lines unknown behavior. Moving from left to right corresponds to decreasing period. There are four bifurcation points: I_C^{AS1}, I_C^{AS2}, I_C^{AS3}, and I_C^S.

away from $\phi = 0$. For each T bifurcation point in Figure 4, there is a corresponding I bifurcation point, which we label I_C^{AS1}, I_C^{AS2}, I_C^{AS3}, and I_C^S.

The bifurcation diagram for large spikes is shown in Figure 5. In this case, the period decreases with increasing phase (i.e., for a fixed I, AS has a shorter period than the third mode, which has a shorter period than S). Thus, increasing I will almost lead to the same bifurcation sequence as decreasing T. We simply reverse the plot in Figure 4. The one difference is that for very large I beyond the bifurcation point T_C^{AS3}, AS cannot bifurcate to the third mode because the latter has a longer period and may not exist at the bifurcation point. AS may lose stability to a nonperiodic or nonphase-locked state that our analysis does not consider.

The situation changes for the bifurcation diagram for small spikes (δ_c small), which is shown in Figure 6. In this case, for fixed parameters, S has a shorter period than the third mode and AS. The bifurcation picture given in Figure 4 breaks down since the S state cannot bifurcate into the third mode if the third mode does not exist at that parameter. The third mode could exist for higher values of I, but it may not be connected to S through a simple bifurcation. There may also be nonperiodic or nonphase-locked behavior. At very large I, AS could possibly exist and bifurcate into the third mode. However, the sufficient conditions for stable AS are not satisfied in this regime.

Recall from the previous two sections that the critical points T_C move toward larger values as δ_c and Δ are increased (except for $T_C^{AS2} = 2\Delta$, which changes only with changing Δ). This implies that the corresponding critical points in the I diagram (I_C) move toward lower values. Thus, for larger δ_c and Δ, the bifurcation points have lower values of I if the spikes are large and higher values if the spikes are small. The bifurcation sequences for g

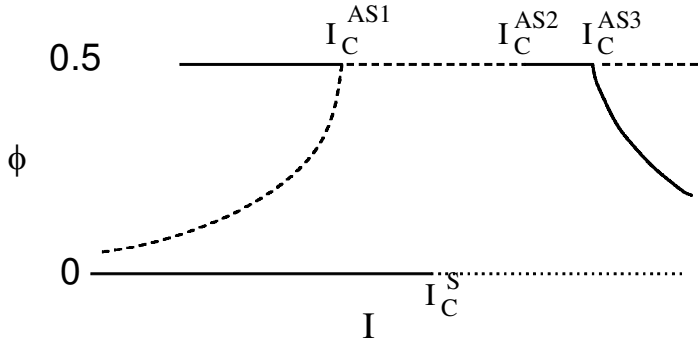

Figure 6: Bifurcation sequence for phase-locked states with phase ϕ and applied current I for small spikes. Solid lines indicate stable states, dashed lines unstable, and dotted lines unknown behavior.

can be deduced by examining Figures 5 and 6. As the gap junction strength g is increased fairly strongly for g, the critical points T_C will decrease (I_C will increase). Thus, the bifurcations occur at a higher value of I. Hence, the region for stable S increases. The region in which the necessary condition for AS stability is satisfied increases in the low I regime. However, as discussed in section 3.3, AS also loses existence at lower I. Thus, for very strong g, only S will exist stably. As g is decreased, the state can bifurcate into AS or third mode depending on the value of I.

3.8 Adding Heterogeneity. With the addition of heterogeneity, the locking condition (see equation 3.3) shows that neither S nor AS is a solution. However, it was shown in Chow (1998) that near synchrony and near antisynchrony are possible for weak enough heterogeneity. As long as $G'(\phi, T)$ is positive at the phase-locked solution, then stability is possible. The stronger the gap junction is, the more likely the two neurons will synchronize. This is expected heuristically but can also be seen from the behavior of $G(\phi, T)$.

Recall from equation 3.4 that $G(\phi, T)$ is constructed from a sum over $\gamma_c(t)$ at periodic intervals. As the gap junction strength increases, $\gamma_c(t)$ begins to look more and more like $\eta_+(t)$, which has positive slope everywhere. Since $\dot{\gamma_c}(0) = 0$, it does not contribute to stability of the synchronous state of $\phi = 0$. However, $\dot{\gamma_c}(t)$ increases with t for the duration of the spike. This can cause $G(\phi, T)$ to rise fairly steeply for $\phi > 0$. So for ϕ near to but away from zero, the spike contributes positively to $G'(\phi, T)$. This also implies that a fast-rising spike may also make synchrony easier to maintain in the presence of heterogeneity.

3.9 Application to Biophysical Neuron Models. We compared the predictions of our analysis on the integrate-and-fire model to biophysical con-

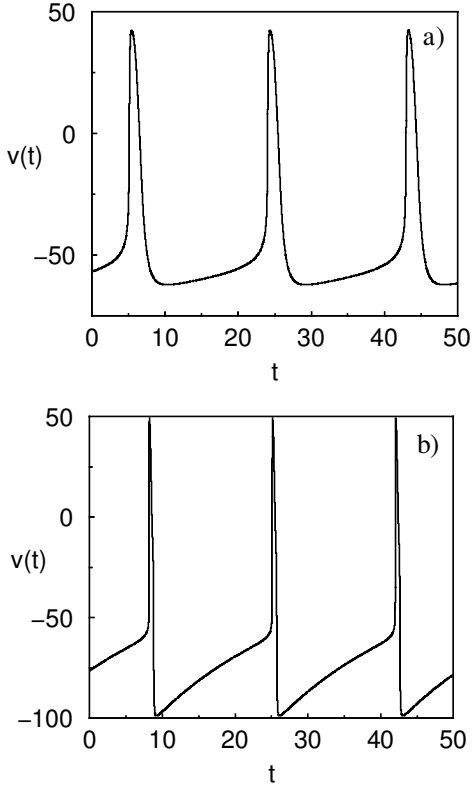

Figure 7: (a) Voltage trace for the interneuron model with $\tilde{I} = 0$. (b) Voltage trace for the reduced Traub-Miles model with $\tilde{I} = 2.0$.

ductance-based neuron models. We considered two different models that represented ranges of possible spike shapes. Figure 7 show examples of the spike forms for an interneuron model of White, Chow, Ritt, Soto-Trevino, and Kopell (1998) and a reduced Traub-Miles (RTM) model (Traub, Jefferys, & Whittington, 1997; Ermentrout & Kopell, 1998). The dynamical equations are given in the appendix. The interneuron model has a wider spike and a larger spike (the size of the spike is in reference to a postspike hyperpolarization) compared to the RTM model. This implies that the interneuron model has a larger δ_c than the RTM model. In the RTM model, the spiking currents play a very small role in the recovery phase, and so a passive decay to threshold is a good approximation. However, for the interneuron model, the spiking currents seem to play an important role in the recovery. From the figures, it appears that the effective leak time of the interneuron model is longer than the RTM model. Recall that time has been scaled by the leak

Table 1: Table of Period T and Stable States for the Interneuron Model with $g = 0.025$ as a Function of Varying Applied Current T.

I	T	State
< -0.55	> 68.1	S (only)
-0.55–1.65	68.1–9.6	S
	24.0–7.7	AS
1.65–19.0	9.6 – 3.4	S
19.0–23.0	3.4 – 3.1	Third mode
> 23.0	< 3.1	AS
25.0	2.7	AS
> 25.4		Nonperiodic

time in the analysis. Thus, for a fixed period, lengthening the leak time (i.e., reducing the leak rate) effectively shortens the scaled period. We looked for steady-state behavior over a range of applied currents I and gap junction conductances g, and ran for many hundreds of periods to ensure that the observed states were not transient.

We first summarize the analysis of our simplified model. For very strong gap junctions, synchrony is the only state that can exist. For weak gap junctions, a bifurcation sequence can be observed as the applied current is changed. The bifurcation sequence will be different for large and small spikes, as seen in Figures 5 and 6. We predict that the interneuron model should behave like a large spike cell and the RTM model should behave like a small spike cell. From section 3.2, we predict that increasing the gap junction strength should decrease the period of AS for the interneuron model since the effective leak time of the interneuron model is long and δ_c is large. On the other hand, it should increase the RTM period since the leak time is short and δ_c is small. The same arguments also predict that for a fixed set of neuronal parameters, the period of S will be longer than the period of AS for the interneuron model, but the opposite will hold for the RTM model.

For the interneuron model with weak coupling ($g = 0.025$), we numerically found a bifurcation sequence (see Table 1) that matched our analytical results. For low levels of applied current, only the synchronous (S) state could be found. At a current of $I = -0.55$, AS appeared. S and AS coexisted for $-0.55 \leq I < 1.65$. An example of AS in the bistable regime is shown in Figure 8. At $I = 1.65$, AS lost stability. S persisted with increasing current until $I = 19$, where it bifurcated into a stable third mode, as seen in Figure 9. The phase difference of the third mode approached $\phi = 0.5$ until $I = 23$, when it bifurcated into AS. Figure 10 shows the voltage traces for AS and $\tilde{I} = 25$. At $I \simeq 25.4$, AS lost stability to a nonperiodic state (see Figure 11).

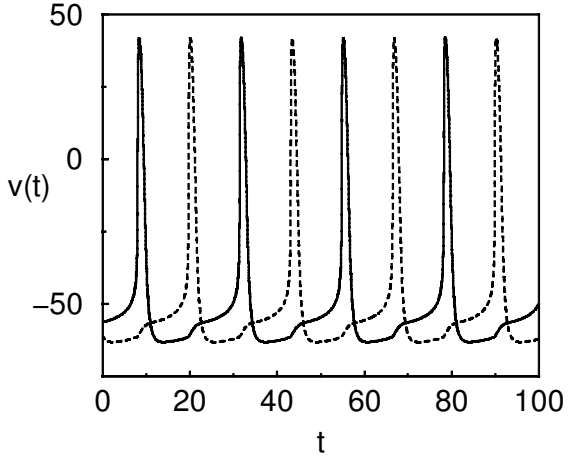

Figure 8: Interneuron model: Antisynchrony in the bistable regime, $g = 0.025$, $\tilde{I} = -0.55$, $T = 24$ ms.

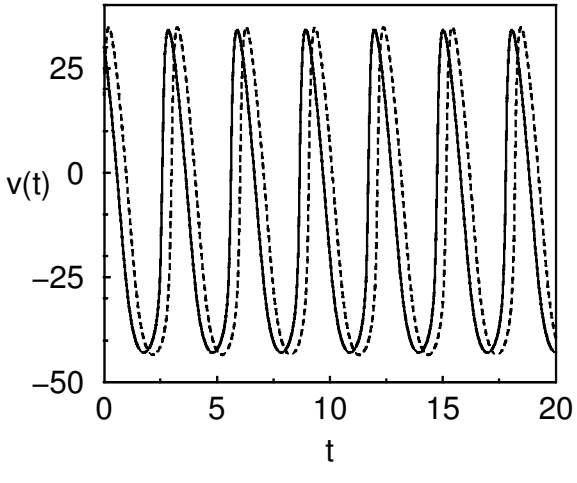

Figure 9: Interneuron model: Third mode, $g = 0.025$, $\tilde{I} = 23$, $T = 3.1$.

Although they are difficult to perceive in the figure, the amplitudes of the spikes are slowly increasing and decreasing.

As the gap junction strength was increased in any of the above states, the cells fell into S, as expected. The period of AS was always shorter than S in the bistable regime, also as expected. In the bistable regime, the periods differed

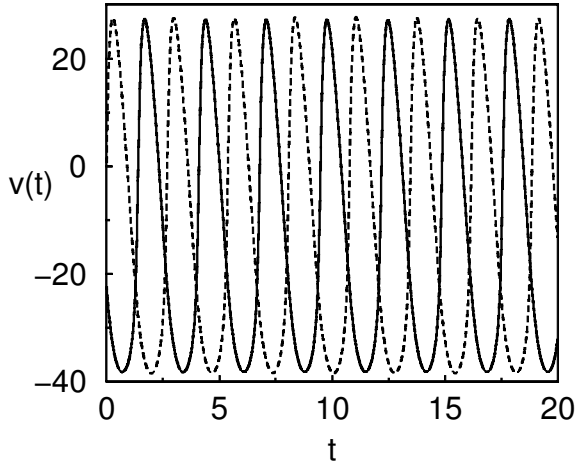

Figure 10: Interneuron model: Antisynchrony in the high-frequency regime, $g = 0.025$, $\tilde{I} = 25$, $T = 2.7$.

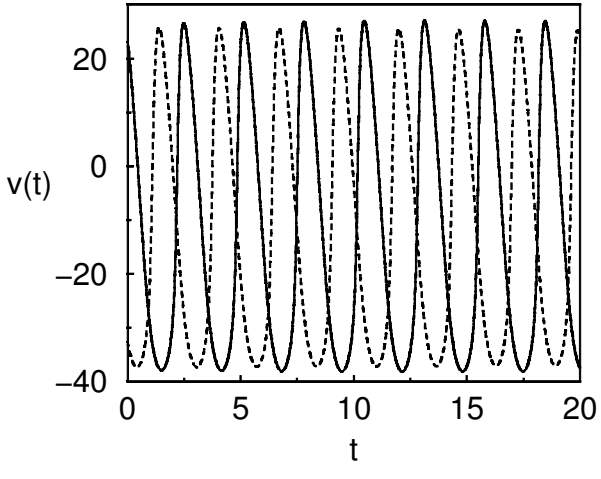

Figure 11: Interneuron model: Nonperiodic state in the high-frequency regime, $g = 0.025$, $\tilde{I} = 25.4$.

roughly by about 20%. Increasing the gap junction strength shortened the AS period, also as predicted (see Figure 12).

The bifurcation sequence for the RTM model with weak coupling ($g = 0.01$) is given in Table 2. For very low currents, only the synchronous state

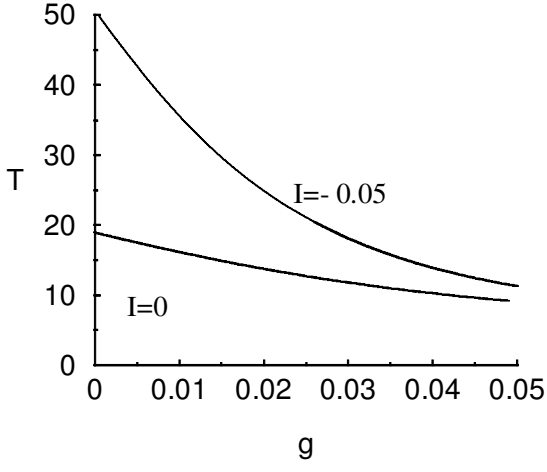

Figure 12: AS period as a function of the gap junction strength for the interneuron model. The S period has the value of 19.0 for $I = 0$ and 50.8 for $I = -0.05$ and does not change with g. AS has a shorter period than S for a fixed I and g.

Table 2: Table of Period T and Stable States for the RTM Model with $g = 0.01$ as a Function of Varying Applied Current T.

I	T	State
< 0.08	> 114	S (only)
0.08–0.55	158–42	AS
	114–39	S
> 0.55	< 39	S
Very large		Non-S

Note: The non-S behavior found at very high I was for smaller values of g.

existed. At $\tilde{I} = 0.08$ and a period of $T = 158$ ms, the AS state came into existence and both S and AS were stable. Figure 13 shows an example of the AS state. At $\tilde{I} = 0.55$ the AS state became unstable. Our numerics for the RTM model found that synchrony extended to very high frequencies. This was to be expected since the spike was extremely narrow. (We note that the sufficient conditions for stable AS are not satisfied for $T < \Delta$, so AS need not be observed at high frequencies.) In our analytical model, the width Δ corresponds to the time for the spike to reach the peak from

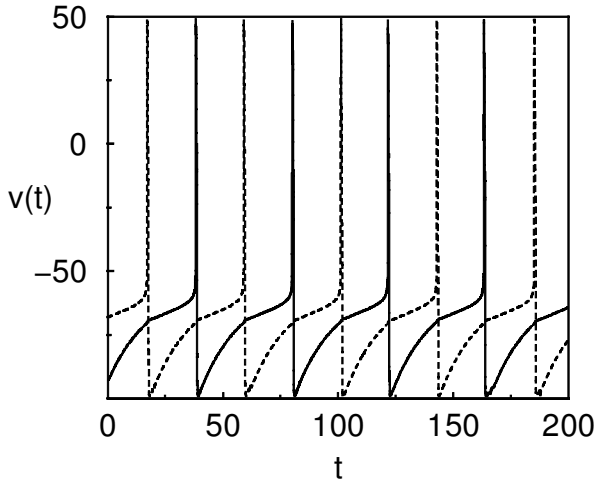

Figure 13: Reduced Traub–Miles model: Antisynchrony in the bistable regime, $g = 0.01$, $\tilde{I} = .55$, $T = 42$ ms.

threshold. For the RTM model, this was on the order of 0.1 ms, which would require a biologically improbable period near $T \simeq 0.2$ or 5000 Hz. On the other hand, the time spent above threshold for the spike was approximately 0.5 ms, which would require $T \simeq 1$ ms or 1000 Hz. We were unable to drive the RTM model fast enough for S to lose stability. At very high applied current ($I \simeq 1370$, $T \simeq .8$ ms), a Hopf bifurcation took place, and continuous spiking was replaced by steady state. (This is often observed in conductance-based models but does not occur in our analytical model.) However, when we lowered the gap junction strength to $g = 0.0001$, we were able to find nonsynchronous behavior for very large I. Figure 14 shows a third mode state for $I = 1000$.

In the bistable regime, the AS period was longer than the S period, opposite of the interneuron model, and the predicted result for small spikes (i.e., δ_c small). The periods between S and AS differed roughly by about 10%. Increasing the gap junction strength increased the period of the AS state, also as expected (see Figure 15).

4 Larger Networks

We consider an all-to-all coupled network of N neurons with gap junctions. Although this is probably unrealistic for very large N, it does serve to gain some qualitative understanding of large network effects. We consider the

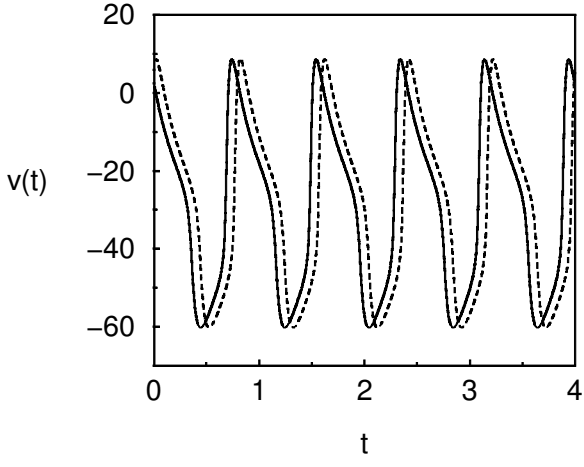

Figure 14: Reduced Traub–Miles model: Third mode for $g = 0.0001$, $\tilde{I} = 1000$, $T = 5.761$ ms.

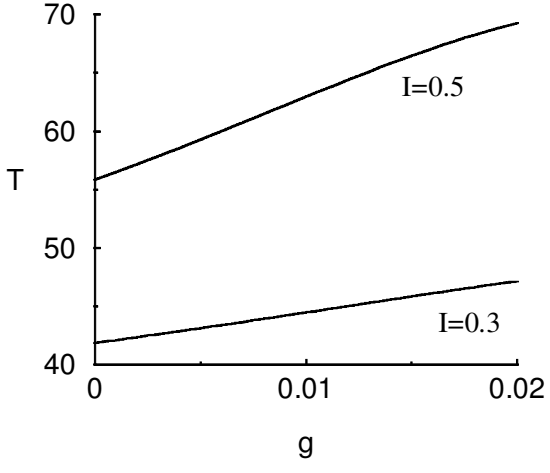

Figure 15: AS period as a function of the gap junction strength for the RTM model. The S period has the value of 41.8 for $I = 0.3$ and 55.8 for $I = 0.5$. AS has a longer period than S.

model

$$\frac{dv_i}{dt} = I - v_i - g\sum_{j\neq i}(v_i - v_j) + \sum_l A(t - t_i^l), \tag{4.1}$$

where i is the neuron index. We consider a network of homogeneous neurons, although the analysis can be done as well with heterogeneous applied currents. We rewrite equation 4.1 in the form of a matrix equation,

$$\frac{d\vec{v}}{dt} = \mathcal{M} \cdot \vec{v} + \vec{f}, \tag{4.2}$$

where

$$\vec{v} = \begin{pmatrix} v_1 \\ v_2 \\ \vdots \\ v_N \end{pmatrix}, \qquad \vec{f} = \begin{pmatrix} I + \sum_l A(t - t_1^l) \\ I + \sum_l A(t - t_2^l) \\ \vdots \\ I + \sum_l A(t - t_N^l) \end{pmatrix} \tag{4.3}$$

and

$$\mathcal{M} = \begin{pmatrix} -1 - (N-1)g & g & \cdots & g \\ g & -1 - (N-1)g & \cdots & g \\ \vdots & \vdots & & \vdots \\ g & g & \cdots & -1 - (N-1)g \end{pmatrix}. \tag{4.4}$$

Proceeding as we had for two neurons, we diagonalize system 4.2. Due to the high degree of symmetry, the matrix $\mathcal{M}$ has only two distinct eigenvalues: -1 and $-1 - Ng$ (which is $N - 1$ times degenerate). Transforming to the diagonalized system, integrating, and transforming back gives us the spike response form

$$v_i(t) = I + \sum_l \Gamma_s(t - t_i^l) + \sum_{j \neq i} \sum_m \Gamma_c(t - t_j^l), \tag{4.5}$$

where

$$\Gamma_s(t) = \eta_+(t) + (N-1)\eta_-(t) \tag{4.6}$$

$$\Gamma_c(t) = \eta_+(t) - \eta_-(t). \tag{4.7}$$

The kernel $\eta_+(t)$ is identical to the two-neuron network kernel (see equation 2.14), and $\eta_-(t)$ has the same form but with $r_- = 1 + Ng$. The equations are similar to those of the N neuron synaptically coupled neuronal network studied in Chow (1998).

We now consider periodic phase-locked states in a network of homogeneous neurons. Suppose the neurons fire at $t_i^l = \phi_i - lT$. At threshold they satisfy the condition

$$1 = I + \sum_l \Gamma_s(lT) + \sum_{j,m} \Gamma_c(mT + (\phi_i - \phi_j)T). \tag{4.8}$$

Due to the permutation symmetry of the neuron index, any symmetric combination of the phases is a possible phase-locked periodic solution (Chow, 1998). Examples include the synchronous state where all the neurons fire together, antisynchrony where half the neurons fire and then the other half fires, the splayphase state where the neurons fire periodically in sequence, and clustered states.

The synchronous solution always exists if the driving current is above threshold. The period is given by the single neuron period. The analysis for the existence of the antisynchronous solution follows as in the two-neuron case. We now examine conditions under which the splay-phase solution can exist. The splay-phase state is defined by $\phi_i = iT/N$, where i varies from 0 to $N-1$. The splay-phase state can exist if a solution for the period T can be found for

$$1 = I + \sum_{l\geq 1} \Gamma_s(lT) + \sum_{j,m\geq 1} \Gamma_c\left(mT - \frac{j}{N}T\right). \tag{4.9}$$

For simplicity, suppose the spikes are separated by at least Δ (i.e., spikes do not overlap). Then

$$\Gamma_s(t) = -e^{-(t-\Delta)} - (N-1)\delta_c e^{-r(t-\Delta)}, \tag{4.10}$$

$$\Gamma_c(t) = -e^{-(t-\Delta)} + \delta_c e^{-r(t-\Delta)}. \tag{4.11}$$

We may now substitute this into equation 4.9 and sum the resulting geometric series to obtain

$$I - 1 = \frac{e^{\Delta}}{e^{T}-1} + \frac{e^{\Delta}}{e^{T/N}-1} + (N-1)\delta_c \frac{e^{r\Delta}}{e^{rT}-1} - \delta_c \frac{e^{r\Delta}}{e^{rT/N}-1}. \tag{4.12}$$

The period of the splay-phase state is given by the smallest solution of T to equation 4.12. For a fixed N, a solution can always be found for some I and T. However, there will be a maximum period that can sustain the splay phase due to the fast threshold modulation effect, as described for antisynchrony in section 3.1, that is, the neurons must remain subthreshold when the other neurons fire.

The sufficient conditions for stability are that $\dot{\Gamma}_c(mT - \frac{j}{N}T) > 0$, for all m and j (Chow, 1998). Thus the separation between the neurons must exceed $t_{\min}$ from equation 3.24 to ensure stability. This sets a minimum period of $T = Nt_{\min}$. It also suggests that there is a region of allowed periods for stable splay phase. If the period is too short, the state loses (sufficient condition for) stability, and if the period is too long, it loses existence. The allowed period for the splay-phase must also scale with the number of neurons in the network N since the separation between the neurons must remain relatively constant independent of network size. This means that the applied

current must be reduced as N increases in order to sustain a stable splay-phase state. Numerical simulations of the interneuron model confirmed these observations. We simulated networks up to $N = 8$ and found the existence of the splay-phase state only over a midrange of periods.

5 Discussion

5.1 Related Modeling Work. The first articles to point out that electrical coupling can be antisynchronizing were by Sherman and Rinzel (1992) and Sherman (1994) using simulations done in the context of pancreatic beta cells, which have bursting electrical behavior. Later work on this system (de Vries, Zhu, & Sherman, 1998) used the fact that the envelopes of the bursts were roughly sinusoidal in shape and used an analysis near a Hopf bifurcation to see how the coupling could destabilize synchrony. Two other papers (Han, Kurrer, & Kuramoto, 1995, 1997) showed that electrical coupling can give rise to antisynchronous solutions if the components of the cells have trajectories close to a homoclinic bifurcation.

The analysis that we do in this article concerns networks of spiking neurons, focusing on the shapes of the spikes. The most similar work deals with excitatory and inhibitory chemical synapses, using the spike response method (Gerstner & van Hemmen, 1992; Gerstner, 1995; Gerstner et al., 1996; Chow, 1998). These and other related models (van Vreesijk et al., 1994; Hansel et al., 1995; Bressloff & Coombes, 1998, 1999) showed that for integrate-and-fire models, inhibitory synapses can stabilize synchrony (provided the timescales of rise and fall of the synapse are slow enough), while excitation generally destabilizes the synchronous solution. (See also Terman, Kopell, & Bose, 1998, and Bose, Terman, & Kopell, in press) for related results about inhibition and excitation in bursting neurons.) One way to understand intuitively the result that gap junctions can be antisynchronizing is to think of the effects of the electrical coupling as combining those of excitation and inhibition. To see this, consider the coupling currents for a nonrectified electrical synapse when the spikes are not (yet) synchronous. In the spike phase of the cycle of one cell, the coupling currents to the other cell are depolarizing, acting like excitation; in the postpolarization phase, these currents can be hyperpolarizing (depending on the phase of the other cell). This intuition suggests that wide and tall spikes should help to destabilize the synchronous state, whereas a long and deep postpolarization phase should encourage synchrony. This is indeed what the mathematics confirms, producing more details about effects of sizes and shapes as well as rigor. This intuition also suggests why frequency of the network plays a role in synchronization: as the frequency increases, the size of the interspike interval decreases much more than any change in the shape of the spike, favoring the effects of the spike over those of the postpolarization phase and thus favoring destabilization of the synchronous solution. This argument shows that one should not expect frequency to play an important role in the

stability of sinusoidal like oscillators coupled electrically.

There are several other articles on electrically coupled neurons (or compartments) that are related to the current work. Kepler, Marder, and Abbott (1990) considered the electrical coupling of a bursting cell and a passive cell to show that the coupling may increase or decrease the frequency of the oscillation, depending on the shape of the waveform of the oscillator. Kopell, Abbott, and Soto-Trevino (1998) showed that if one of the elements of the network is bistable and the other is an oscillator, the network can exhibit much greater complexity; they introduced new geometric techniques very different from the ones in this article or in Kepler et al. (1990). Manor, Rinzel, Segev, and Yarom (1997) showed that cells with heterogeneous properties, none of them oscillators, could produce an oscillation in an electrically coupled system that is the appropriate average of the dynamics. Electrical coupling is also relevant to understanding the dynamics of compartmental models in which the conductances vary between compartments (Booth & Rinzel, 1995; Li, Bertram, & Rinzel, 1996; Mainen & Sejnowski, 1996; Pinsky & Rinzel, 1994).

Finally, we point out that the literature on neural oscillators is large and rapidly growing, so the above list constitutes only the work that is most directly related to the themes of this article. Ritz and Sejnowski (1997) provide a review of some recent work on neural oscillators.

5.2 Gap Junctions in Physiological Systems. Gap junctions are found in many tissues of the body, including the nervous system. (For reviews, see Bennett, 1997, and Dermietzel & Spray, 1993.) Even in the nervous system, electrical coupling is found in a wide variety of cells, including astrocytes and oligendrocytes, as well as neurons. Many functions have been attributed to these electrical synapses, including exchanges of metabolites and second messengers, and buffering the K+ activity surrounding active neurons (Dermietzel & Spray, 1993). For neurons, the most common function ascribed to electrical synapses is mediating synchrony among active cells or relaying signals quickly. Although gap junctions are thought to be most prevalent (at least in vertebrates) during early development, they are also known to exist in the adult mammalian central nervous system, for example, in the neocortex (Gibson, Beierlein, & Connors, 1999), the hippocampus (Draguhn, Traub, Schmitz, & Jefferys, 1998), the inferior olive (Llinas, Baker, & Sotelo, 1974), and the retina (Dowling, 1991).

In this article, we have shown that electrical coupling can organize a rhythm to be asynchronous, especially at low coupling strengths. The ability of a collection of spiking neurons to synchronize is dependent on the size and shape of the spike form, as well as the frequency at which the cells are firing. At low coupling strengths and very high firing rates (dependent on the shape of the spike wave form), the synchronized state is unstable, and a pair of cells fires in antisynchrony. For a lower range of frequencies, the synchronized and antisynchronized states are bistable. For a population,

the network behavior can have the phases splaying out over the circle.

One preparation in which there are well-documented gap junctional connections and oscillator cells firing at high rates is the pacemaker nucleus of the weakly electric fish, *Apteronotus* (Dye, 1988, 1991; Moortgat, Bullock, & Sejnowski, 2000a, 2000b). In this tissue, cells fire very precisely, and synchronously (Dye, 1988). Evidence for distribution of phases of the pacemaker cells of that nucleus is given in Figure 8 of Dye (1988). Pharmacological manipulations that increase the internal concentration of Ca^{2+} and are presumed to decrease the strength of the gap junctional coupling (Spray & Bennett, 1985) do partially desynchronize the population; however, the desynchronization may be due to differences in the natural frequencies rather than the ability of the weak coupling to desynchronize actively even identical cells, as discussed above. In contrast to Dye (1991), Moortgat et al. (2000a) observe that adding gap junction blockers results in a general reduction of the frequency of oscillation of the pacemaker nucleus. This is predicted above for the model with large spikes.

Gap junctions have recently been documented within two distinct subsets of interneurons in the rat neocortex (Gibson et al., 1999), one of which (the fast-spiking interneurons) gets strong inputs from the thalamus. In recent work, Gibson and Beierlein (pers. comm.) have injected depolarizing current into pairs of electrically coupled fast-spiking interneurons to modulate their frequency. In one pair of cells at a frequency of 40 Hz, the pair oscillated synchronously; with further depolarization that caused the frequency of each cell to go up to approximately 100 Hz, the cells fired in antisynchrony. This is in agreement with predictions from our theory. However, other pairs did not show this effect.

Another potential application of this work concerns bursting behavior of interneurons in the hippocampus. In recent simulations of data from the work of Zhang et al. (1998), Skinner, Zhang, Velasquez, and Carlen (1999) investigated a model network of cells coupled by gap junctions and inhibitory synapses. Blocking the inhibition increased the frequency of each of the cells; at the higher frequencies, the spikes within a burst of the electrically coupled cells had an antisynchronous relationship. In a future publication, we will analyze this system and show that one important effect of the inhibition on the network can be to change its frequency, which affects what configurations are stable using the electrical coupling. The techniques used for the analysis are similar to those used in Chow (1998) to analyze the effects of chemical synapses on model neurons. For these neurons, the effects of the chemical and electrical neurons in the spike-response equations are additive. Hence, the same formalism can be used for situations involving both kinds of synapses acting in parallel.

High-frequency spiking is also found in hippocampal interneurons during ripples, and gap junctional coupling is implicated in the coordination of these rhythms (Draguhn et al., 1998). More recent work (Traub, Schmitz, Jefferys, & Draguhn, 1999) suggests that the mechanism of production of the

rhythms involves spontaneous production of spikes in the axons with transmittal through a sparsely connected network of axo-axonal connections. Although the mechanism that produces the frequency in that case is different (it depends on the network connectivity and the spontaneous rate of action potentials), it remains to be understood if the mechanism that produces the coherence of the network is similar to the one described in this article.

In any physiological situation, the network behavior is affected by heterogeneity, spatial structure of the neurons, connectivity of the network, and interaction with chemical synapses. The analysis presented considered only connections between soma and/or axons, in which spatial and delay effects are not included. For dendro-dendritic connections, such delays would be important. Although it is not within the scope of this article to present the complete analysis, we report here that a similar (but more complicated) analysis of neurons connected with gap junctions at the end of a passive dendrite leads to a change in parameter ranges in which different configurations are stable. In particular, the regime in which asynchrony is stable is greatly increased and that in which synchrony is stable is reduced. We believe that this is due to the filtering properties of the dendrite, which changes the shape of the spike at the synapse.

Ability to fire in an asynchronous way increases the flexibility of network dynamics. This article provides insight into how such asynchrony can be fostered by electrical coupling, even in the absence of the above complexities, all of which create a much richer dynamical environment. It remains to understand how these extra features might interact with the mechanisms described in this article to allow flexible modulation of network behavior.

Appendix: Neuron Dynamics

In our simulations, we considered a network of N conductance-based single-compartment neuron models coupled electrically with gap junctions. The membrane potential obeyed the current balance equation,

$$C\frac{dV_i}{dt} = \tilde{I} - I_{Na} - I_K - I_L - \sum_{j\neq i} g(V_i - V_j), \tag{A.1}$$

where i is the neuron index that runs from 1 to N, g is the gap junction conductance, $\tilde{I}$ is the applied current, $I_{Na} = g_{Na}m^3h(V_i - V_{Na})$ and $I_K = g_K n^4(V_i - V_K)$ are the spike-generating currents, $I_L = g_L(V_i - V_L)$ is the leak current, and $C = 1\mu\mathrm{F/cm}^2$.

The interneuron model in White et al. (1998) used the following parameters: $g_{Na} = 30\ \mathrm{mS/cm}^2$, $g_K = 20\ \mathrm{mS/cm}^2$, $g_L = 0.1\ \mathrm{mS/cm}^2$, $V_{Na} = 45$ mV, $V_K = -80$ mV, and $V_L = -60$ mV. The activation variable m was assumed fast and substituted with its asymptotic value $m = m_\infty(v) = (1 +$

$\exp[-0.08(v+26)])^{-1}$. The gating variables h and n obey

$$\frac{dh}{dt} = \frac{h_\infty(v) - h}{\tau_h(v)}, \qquad \frac{dn}{dt} = \frac{n_\infty(v) - n}{\tau_n(v)}, \tag{A.2}$$

with $h_\infty(v) = (1+\exp[0.13(v+38)])^{-1}$, $\tau_h(v) = 0.6/(1+\exp[-0.12(v+67)])$, $n_\infty(v) = (1+\exp[-0.045(v+10)])^{-1}$, and $\tau_n(v) = 0.5+2.0/(1+\exp[0.045(v-50)])$.

The reduced Traub–Miles model (Traub et al., 1997; Ermentrout & Kopell, 1998) used the following parameters: $g_{Na} = 100$ mS/cm^2, $g_K = 80$ mS/cm^2, $g_L = 0.05$ mS/cm^2, $V_{Na} = 50$ mV, $V_K = -100$ mV, $V_L = -67$ mV; $m = m_\infty(v) = \tilde{\alpha}_m(v)/(\tilde{\alpha}_m(v)+\tilde{\beta}_m(v))$, where $\tilde{\alpha}_m(v) = 0.32(54+v)/(1-\exp(-(v+54)/4))$ and $\tilde{\beta}_m(v) = 0.28(v+27)/(\exp((v+27)/5)-1)$;

$$\frac{dn}{dt} = \tilde{\alpha}_n(v)(1-n) - \tilde{\beta}_n(v)n \tag{A.3}$$

with $\tilde{\alpha}_n(v) = 0.032(v+52)/(1-\exp(-(v+52)/5))$, $\tilde{\beta}_n(v) = 0.5\exp(-(v+57)/40)$; $h = h_\infty(v) = \max[1-1.25n, 0]$.

The ODEs were integrated using the CVODE method with the program XPPAUT written by G. B. Ermentrout and available online at http://www.pitt.edu/~phase/.

Acknowledgments

We thank John White and Bard Ermentrout for many helpful discussions. This work was supported by NIH grant K01 MH01508 (CC), NIMH grant 47150 (NK), and NSF grant 9200131 (NK), and the A. P. Sloan Foundation (CC).

References

Bennett, M. (1997). Gap junctions as electrical synapses. *J. Neurocytology, 26*, 349–366.

Booth, V., & Rinzel, J. (1995). A minimal compartment model for a dendritic origin of bistability of motoneuron firing patterns. *J. Comp. Neurosci., 2*, 1–14.

Bose, A., Terman, D., & Kopell, N. (in press). Almost-synchronous solutions in networks of neurons for mutually coupled excitatory synapses. *Physica D*.

Bressloff, P. C., & Coombes, S. (1998). Desynchronization, mode locking, and bursting in strongly coupled integrate-and-fire oscillators. *Phys. Rev. Lett., 81*, 2168–2171.

Bressloff, P. C., & Coombes, S. (2000). Dynamics of strongly coupled spiking neurons. *Neural Comp., 12*, 91–129.

Chow, C. C. (1998). Phase-locking in weakly heterogeneous neuronal networks. *Physica D, 118*, 343–370.

Chow, C. C., White, J. A., Ritt, J., & Kopell, N. (1998). Frequency control in synchronous networks of inhibitory neurons. *J. Comp. Neurosci., 5*, 407–420.

Dermietzel, R., & Spray, D. (1993). Gap junction in the brain: Where, what type, how many and why? *TINS, 16*, 186–192.

de Vries, G., Zhu, H.-R., & Sherman, A. (1998). Diffusively coupled bursters: Effects of heterogeneity. *Bull. Math. Biol., 60*, 1167–1200.

Dowling, J. E. (1991). Retinal neuromodulation: The role of dopamine. *Visual Neuroscience, 7*, 87–97.

Draguhn, A., Traub, R. D., Schmitz, D., & Jefferys, J. G. R. (1998). Electrical coupling underlies high-frequency oscillations in the hippocampus *in vitro*. *Nature, 394*, 189–192.

Dye, J. (1988). An in vitro physiological preparation of a vertebrate communicatory behavior: Chirping in the weakly electric fish, *Apteronotus. J. Comp. Physiol. A, 163*, 445–458.

Dye, J. (1991). Ionic and synaptic mechanisms underlying a brainstem oscillator: An in vitro study of the pacemaker nucleus of *Apteronotus. J. Comp. Physiol A, 168*, 521–532.

Ermentrout, G. B., & Kopell, N. (1998). Fine structure of neural spiking and synchronization in the presence of conduction delays. *Proc. Nat. Acad. Sci. USA, 95*, 1259–1264.

Gerstner, W. (1995). Time structure of the activity in neural network models. *Phys. Rev. E, 51*, 738–758.

Gerstner, W., & van Hemmen, J. L. (1992). Associative memory in a network of "spiking" neurons. *Network, 3*, 139–164.

Gerstner, W., van Hemmen, J. L., & Cowen, J. (1996). What matters in neuronal locking? *Neural Comput., 8*, 1653–1676.

Gibson, J. R., Beierlein, M., & Connors, B. (1999). Two networks of electrically coupled neurons in the neocortex. *Nature, 402*, 75–79.

Han, S. K., Kurrer, C., & Kuramoto, Y. (1995). Dephasing and bursting in coupled neural oscillators. *Phys. Rev. Lett., 75*, 3190–3193.

Han, S. K., Kurrer, C., & Kuramoto, Y. (1997). Diffusive interaction leading to dephasing of coupled neural oscillators. *Int. J. Bifurcations and Chaos, 7*, 869–876.

Hansel, D., Mato, G., & Meunier, C. (1995). Synchrony in excitatory neural networks. *Neural Comput., 7*, 307–337.

Kepler, T. B., Marder, E., & Abbott, L. F. (1990). The effect of electrical coupling on the frequency of model neuronal oscillators. *Science, 6*, 83–85.

Kopell, N., Abbott, L. F., & Soto-Trevino, C. (1998). On the behavior of a neural oscillator electrically coupled to a bistable element. *Physica D 121*, 367–395.

Li, Y.-X., Bertram, R., & Rinzel, J. (1996). Modeling N-methyl-D-aspartate–induced bursting in dopamine neurons. *Neuroscience, 71*, 397–410.

Llinas, R., Baker, R., & Sotelo, C. (1974). Electrotonic coupling between neurons in the cat inferior olive. *J. Neurophysiol., 37*, 560–571.

Mainen, Z. F., & Sejnowski, T. J. (1996). Influence of dendritic structure on firing pattern in model neocortical neurons. *Nature, 382*, 363–366.

Manor, Y., Rinzel, J., Segev, I., & Yarom, Y. (1997). Low amplitude oscillation in the inferior olive: A model based on electrical coupling of neurons with heterogeneous channel densities. *J. Neurophysiol., 77*, 2736–2752.

Moortgat, K. T., Bullock, T. H., & Sejnowski, T. J., (2000a). Precision of the pacemaker nucleus in a weakly electric fish: network vs. cellular influences. *J. Neurophysiol., 83*, 971–983.

Moortgat, K. T., Bullock, T. H., & Sejnowski, T. J. (2000b). Gap junction effects on precision and frequency of a model pacemaker network. *J. Neurophysiol., 83*, 984–997.

Pinsky, P. F., & Rinzel, J. (1994). Intrinsic and network rhythmogenesis in a reduced Traub model for CA3 neurons. *J. Comp. Neurosci., 1*, 39–60.

Ritz, R., & Sejnowski, T. J. (1997). Synchronous oscillatory activity in sensory systems: New vistas on mechanisms. *Current Opinion in Neurobiology, 7*, 536–546.

Sherman, A. (1994). Anti-phase, asymmetric and aperiodic oscillations in excitable cells—I. Coupled bursters. *Bull. Math. Biology, 56*, 811–835.

Sherman, A., & Rinzel, J. (1992). Rhythmogenic effects of weak electrotonic coupling in neuronal models. *Proc. Natl. Acad. Sci. U.S.A., 89*, 2471–2474.

Skinner, F. K., Zhang, L., Velasquez, J. L. P., & Carlen, P. L. (1999). Bursting in inhibitory interneurons: A role for gap-junctional coupling. *J. Neurophysiol., 81*, 1274–1283.

Somers, D., & Kopell, N. (1993). Rapid synchronization through fast threshold modulation. *Biol. Cybern., 68*, 393–407.

Spray, D. C., & Bennett, M. V. (1985). Physiology and pharmacology of gap junctions. *Annu. Rev. Physiol., 47*, 281–303.

Terman, D., Kopell, N., & Bose, A. (1998). Dynamics of two mutually coupled slow inhibitory neurons. *Physica D, 117*, 241–275.

Traub, R. D., Jefferys, J. G. R., & Whittington, M. A. (1997). Simulation of gamma rhythms in networks of interneurons and pyramidal cells. *J. Comp. Neurosci., 4*, 141–150.

Traub, R. D., Schmitz, D., Jefferys, J. G. R., & Draguhn, A. (1999). High-frequency population oscillations are predicted to occur in hippocampal pyramidal neuronal network interconnected by axo-axonal gap-junctions. *Neuroscience, 92*, 407–426.

van Vreeswijk, C., Abbott, L., & Ermentrout, G. B. (1994). When inhibition not excitation synchronizes neural firing. *J. Comp. Neurosci., 1*, 313–321.

White, J. A., Chow, C. C., Ritt, J., Soto-Trevino, C., & Kopell, N. (1998). Synchronization and oscillatory dynamics in heterogeneous, mutually inhibited neurons. *J. Comp. Neurosci., 5*, 5–16.

Zhang, Y., Velazquez, J. L. P., Tian, G. F., Wu, C. P., Skinner, F. K., Carlen, P. L., & Zhang, L. (1998). Slow oscillations ($\leq$ 1 Hz) mediated by GABAergic interneuronal networks in rat hippocampus. *J. Neurosci., 18*, 9256–9268.

Received January 29, 1999; accepted September 2, 1999.